Friction

Research Article

The influence of sliding velocity and temperature on the ductile-to-brittle transition in asperity-level wear: A molecular dynamics study

Sacha Zenon Wattel✉, Jean-François Molinari

Cite this article: Wattel SZ, Molinari J-F. *Friction* 2026, **14**(6): 9441212. https://doi.org/10.26599/FRICT.2025.9441212

ABSTRACT: During sliding contact, asperities may undergo either ductile smoothing or brittle fracture, producing debris. A critical junction scale, d^*, governed by material properties, dictates this transition. Previous studies using molecular dynamics (MD) simulations with tunable interatomic potentials revealed this scale under quasi-static conditions—fixed temperature and low sliding velocities. Here, we extend that work to investigate how temperature and sliding velocity influence the ductile-to-brittle transition at the asperity level. Material properties governed by short-range atomic interactions, such as stiffness and surface energy, remain relatively constant with temperature. In contrast, shear strength, influenced by longer-range interactions, decreases with rising temperature, promoting a brittle-to-ductile shift in asperity behavior. Incorporating temperature-dependent shear strength into the d^* expression successfully predicts the lower bound of the transition. However, capturing the upper bound requires an additional term to account for ductile fracture energy. At higher sliding velocities, a new brittle failure mode emerges: Instead of a single crack forming at the asperity base, multiple dynamically propagating cracks develop, resulting in fragmented debris. Finally, long-time scale MD simulations of rough-on-rough contact under adiabatic conditions reveal how interface heating influences wear during extended sliding. Regardless of velocity, asperities initially fracture and generate debris that aggregates into a single rolling particle. This particle grows steadily until the surrounding material nears its liquefaction temperature, triggering collapse. These simulations reproduce known wear regimes: an early, high-wear running-in phase followed by a steady-state mild wear stage. Notably, tangential work, heat generation, and wear rate depend primarily on total sliding distance rather than velocity.

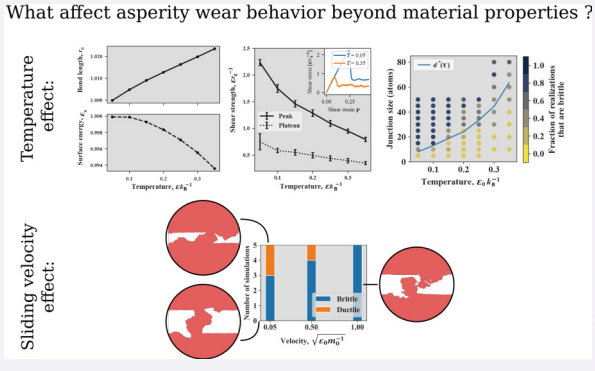

KEYWORDS: molecular dynamics; tribology; wear; temperature; sliding velocity; ductile-to-brittle transition

1 Introduction

Almost any surface, when observed from close enough, is rough. When two surfaces are pressed against each other, the contact does not happen through the entire apparent contact area but rather, due to the roughness, on micro-contacts happening between asperities. As such, any phenomena happening at the interface between two surfaces, such as friction, wear, or adhesion, is dictated by the behavior of these micro-contacts.

During sliding experiments, when two asperities collide, two main behaviors have been observed: Sometimes asperities undergo large plastic deformation and the surfaces gradually smoothen [1–8], whereas, in other experiments, the asperities fracture and detach [4, 9, 10].

In recent years, there has been a stream of research using molecular dynamics (MD) simulations to study the tribological behavior of rough surfaces at the asperity level. In these simulations, a family of interatomic potentials whose ductility can be tuned is used. Thanks to these potentials, a single numerical model could capture both experimentally-observed behaviors of asperity collision [11]. A length scale, the critical junction size d^*, coming from an energy argument comparing elastic strain energy to the critical energy release rate, was formulated to predict the ductile-to-brittle transition. When asperities collide, they create a junction, a micro-contact, and deform, accumulating elastic strain energy. Then, asperities may detach only if the stored strain energy becomes larger than the energy necessary to create cracks at the base of the asperities. This transition happens at the critical junction size d^*. If the micro-contact size remains below d^*, the asperities deform plastically. However, if the contact reaches a size comparable to d^*, cracks appear and the asperities detach. For brittle material, the critical junction size d^* is expressed as [11]:

Civil Engineering Institute, Materials Science and Engineering Institute, Ecole Polytechnique Fédérale de Lausanne (EPFL), Lausanne 1015, Switzerland.

✉ Corresponding author. E-mail: sacha.wattel@epfl.ch

Received: July 9, 2025; Revised: November 30, 2025; Accepted: December 31, 2025

$$d^* = f\frac{4\gamma_{surf}\mu}{\tau_{el}^2} \quad (1)$$

where γ_{surf} is the surface energy; μ is the shear modulus; τ_{el} is the elastic shear strength; f is a geometry factor capturing the shape of the asperity, the path of the fracture and the area plastified (of the order of unity [11, 12]).

Among further studies, the critical junction size d^* has been found to still apply to different problems such as the adhesive wear of heterogeneous materials [13], the abrasive wear with rolling debris under different normal pressures [14] or the cutting mechanism during machining [15, 16]. It was also linked to another length scale, the fracture process zone size [17] to explain why breaking asperities much larger than d^* requires less frictional work [18]. Finally, a recent line of work has focused on finding first principles-based predictions of wear at the macro scale, obtaining a qualitative agreement with Archard's law [19, 20] or a distribution for wear particle size of rubber comparable to the one observed in experiments [21].

While all these studies show the importance of the critical junction size in furthering the understanding of wear, the influence of two important variables on d^* was not yet explored: the temperature and the sliding velocity. The sliding velocity considered would be of low magnitude such that conditions could be described as quasi-static. However, sliding velocity is a key parameter in tribology, as it directly affects the impact speed and frequency of asperity collisions as well as the deformation rate. Both a higher frequency of collisions and a higher rate of deformations lead to a higher rate of heat generation from mechanical work, increasing temperature and changing the mechanical properties of the material. One of the expected effects is that the material will be more ductile at high temperature. In its current formulation, d^* assumes that the material is perfectly brittle by considering only the free surface energy γ_{surf} in the critical energy release rate G_c:

$$G_c = 2\gamma_{surf} \quad (2)$$

This formulation has been found to underestimate the critical junction size for more ductile materials [13]. Indeed, for ductile materials, the critical energy release rate should not only include surface energy but also the energy dissipated as plastic strain near the crack tip and possibly other intrinsic and extrinsic energy dissipation mechanisms, regrouped under the term γ_p:

$$G_c(T) = 2\left(\gamma_{surf}(T) + \gamma_p(T)\right) \quad (3)$$

with T the temperature. As the temperature increases, their material properties may change. As such, the prediction of d^* becomes temperature-dependent:

$$d^*(T) = f\frac{2G_c(T)\mu(T)}{\tau_{el}^2(T)} \quad (4)$$

Higher rates of deformation can also lead to strain localization and a more brittle behavior which would counteract increased material ductility. Finally, previous experiments with atomic force microscopy tips and numerical simulations at the atomic scales suggest that sliding velocity has little impact on wear and friction [22, 23] until a certain threshold above which friction and wear diminish [9, 24]. This threshold corresponds to the moment when, due to its inertia, the tip of the atomic force microscope stops closely following the contour of the surfaces and instead hovers above the surface.

The goal of this work is to study how these competing effects affect the tribological behavior of the material and how the critical junction size can predict the ductile-to-brittle transition at different temperatures and sliding velocities.

To answer these questions, the material properties that enter d^* formulation are measured at different temperatures. Then, two sets of junction shearing simulations are run, one varying the temperature and keeping the velocity constant, the other one varying the sliding velocity while keeping the temperature constant. Finally, rough-on-rough sliding simulations are run for a long time frame in both thermostated and adiabatic, non-thermostated, conditions to observe how the heat generated at the sliding interface affects the tribological behavior over time and sliding distance.

2 Method

All simulations are run using the MD software LAMMPS [25] and are constrained to be two-dimensional in space. Unless otherwise mentioned, all units are rendered dimensionless (reduced units) by taking a reference energy ϵ_0, length r_0 (respectively the depth and distance of the potential well), and atomic mass m_0 as well as a unity Boltzmann constant $k_B = 1$. The resulting reductions are summarized in Table 1.

Tunable model potential. The atomistic simulations use interatomic pair potentials for which short-range and long-range interactions are decoupled and can be tuned individually [26]. This is done by modifying the tail part of the potential without changing the part close to the energy well. Mechanically, this results in the possibility of changing the plastic properties (strength, hardness, etc.) without affecting the elastic ones (stiffness, equilibrium lattice spacing, surface energy, etc.). In doing so, the brittle, fracture-dominated behavior can be favored at computationally-affordable scales [11, 26, 27].

The potential energy can be expressed as

$$\frac{V(r)}{\epsilon_0} = \begin{cases} (1-e^{\alpha(r-r_0)})^2 - 1, & r < 1.1r_0 \\ c_1\dfrac{r^3}{6} + c_2\dfrac{r^2}{2} + c_3 r + c_4, & 1.1r_0 \le r \le r_{cut} \\ 0, & r_{cut} \le r \end{cases} \quad (5)$$

where r is the interatomic distance, ϵ_0 the depth of the well, r_0 the interatomic distance of the bottom of the well, and $\alpha = 3.93\,r_0^{-1}$ a parameter that tunes the stiffness. The tail of the potential can be shortened or elongated with r_{cut}. The parameters c_1, c_2, c_3, and c_4 are chosen to ensure continuity of the potential and its derivative at $r = 1.1r_0$ and $r = r_{cut}$.

Table 1 Table of reductions used to render all quantities dimensionless. These reductions are common within the atomistic simulation community and are sometimes referred to as the Lennard–Jones reduced unit. k_B is the Boltzmann constant. The last column is indicative and gives an equivalent in usual units to the reduced units [49]

Quantity	Reduction	^{56}Fe equivalent
Distance	r_0	2.88 Å
Mass	m_0	55.9 Da
Energy	ϵ_0	0.409 eV
Time	$r_0\sqrt{m_0\epsilon_0^{-1}}$	343 fs
Velocity	$\sqrt{m_0^{-1}\epsilon_0}$	840 ms^{-1}
Force	$\epsilon_0 r_0^{-1}$	0.227 nP
Pressure	$\epsilon_0 r_0^{-3}$	2.74 GPa
Temperature	$\epsilon_0 k_B^{-1}$	4,746 K

One main potential, P_b, is used in this work with $r_{cut} = 1.42r_0$. This potential is particularly brittle with a critical junction size $d^* \approx 10r_0$ at low temperature. This allows for a clear observation of the ductile-to-brittle transition with temperature increase at a reasonably affordable scale.

For rough-on-rough simulations, a second potential with reduced adhesion, $P_{low} = 0.3P_b$, is used to mimic an initial passivation of the surface.

Shear strength. A temperature increase is expected to render a material more ductile. In the frame of the critical junction size, this is reflected by a reduced shear strength leading to a larger d^*. To track how relevant the critical junction size is relative to temperature variation, it is necessary to evaluate d^* at varying temperatures. For this, the shear strength of the material is evaluated at different temperatures. The shear strength is measured as follows: A square box with periodic boundaries is sheared, and the maximum, volume-averaged, virial stress attained is picked as the shear strength, as represented in Fig. 1(a). The temperatures studied range from $T = 0.05$ to $T = 0.35$. The upper bound is chosen so that the material stays solid, the melting point being between $T = 0.4$ and $T = 0.45$. The box is deformed at a shear rate of 0.001 and the time integration is solved via an NVT scheme with a Nose-Hoover thermostat [28, 29] set at the initial temperature and with a time step of 0.005. The shearing is parallel to a weak plane of the lattice. The side of the box is 100-atom long, and its size is a multiple of the lattice constant to avoid initial tension at the periodic boundaries. For each initial temperature, ten realizations of the simulations are run to take into account the stochasticity inherent to finite-temperature atomistic simulations. The shear strength at a given temperature is then the average over the different realizations of the maximal shear virial stress attained.

Critical junction size. The critical junction size is determined at different temperatures with a process similar to the one described in the previous work of Wattel et al. [13]. The simulation domain, pictured in Fig. 1(b), represents two asperities that are in contact and have formed a junction of size d. The size of the domain scales with the size of the junction as indicated in the Fig. 1(b). A pressure $P = 0.3$ is applied on the top and bottom boundary. A velocity $v = 0.015$ is imposed on the top boundary. The lateral boundaries are periodic. A six-atom thick Langevin thermostat layer is placed next to the top and bottom boundaries. For each initial temperature and junction size, five realizations of the simulations are run to take into account the stochasticity inherent to finite-temperature atomistic simulations.

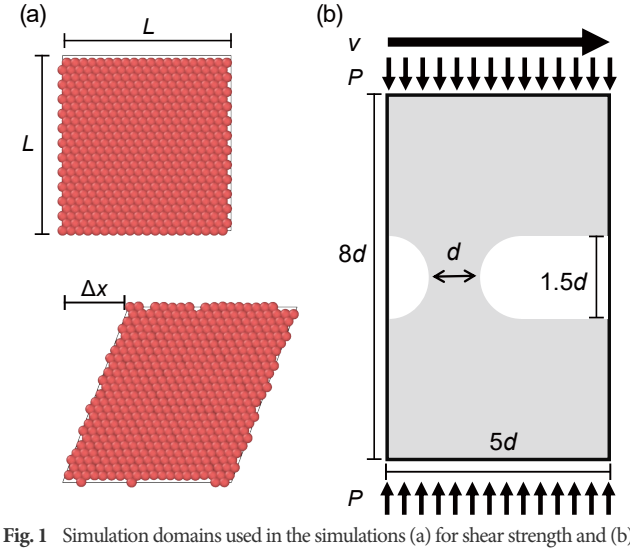

Fig. 1 Simulation domains used in the simulations (a) for shear strength and (b) for critical junction size.

Shear rate effect. To measure the effect of the sliding velocity, simulations similar to the one of the critical junction size are performed. The imposed velocity on the top boundary ranges from $v = 0.05$ to $v = 0.1$. The initial temperature is set at $T = 0.2$ and the junction size at $d = 15$. A velocity field ranging from 0 on the bottom boundary to the imposed velocity v on the top boundary is superimposed on the initial velocity field corresponding to the temperature initialization. This is done to avoid vertical wave propagation from the top boundary. The lateral boundaries are periodic. A six-atom thick Langevin thermostat layer is placed next to the top and bottom boundaries. For each sliding velocity, five realizations of the simulations are run to take into account the stochasticity inherent to finite-temperature atomistic simulations.

Long time frame rolling simulation. The final simulations are long time frame simulations of rough-on-rough surfaces with adiabatic boundary conditions. The simulation domain is a square box of side 500 atoms as represented in Fig. 2. A normal pressure $P = 0.02$ is applied on the top and bottom boundary. The lateral boundary conditions are periodic. The bottom boundary condition is fixed horizontally, and the bottom block is initially at rest. For the thermostated simulations, a six-atom thick Langevin thermostat layer is placed next to the top and bottom boundaries. None is placed for the adiabatic simulations. A velocity $v = 0.05$, $v = 0.25$, or $v = 0.5$ is imposed on the top boundary, and the top block is initialized to the same horizontal velocity v. Initially, the two surfaces are not in contact, but the pressure puts them in contact. The initial temperature is set at $T = 0.05$. As there is no thermostat in the simulation, the temperature can freely rise as mechanical work is converted into heat.

The rough surfaces have self-affine properties and are randomly generated with the software Tamaas [30, 31]. The surfaces have a Hurst exponent of $H = 0.8$, close to natural surfaces [32], and the power spectral density frequencies range from $q_{min} = 3$ to $q_{max} = 50$, meaning the surfaces are composed of three main asperities. Two surfaces are generated, one for the top, one for the bottom, and are scaled to be 100-atom high and placed as pictured in Fig. 2. To reproduce the rough surfaces in the atomistic simulations, a regular hexagonal lattice of atoms is first generated. Then, any atom situated in the gap between the two random surfaces is removed. All three long-time frame simulations start from this same configuration.

Two interatomic potentials are used, the brittle potential P_b and a similar potential with reduced adhesion: $P_{low} = 0.3P_b$. Atoms initially on the surface interact with each other and the bulk atoms through the potential P_{low}. Atoms in the bulk interact with each other through P_b. The number of neighbors of each atom is used to determine which atoms are on the surface. Then, at the first time step, the atoms on the surface are permanently assigned to the surface atom group, and the rest are assigned to be bulk atoms. Without this reduced surface adhesion, the initial contacts between the asperities tend to interact with each other and act as one large contact. As a result, deep cracks propagate to the top and bottom boundary conditions. Reducing the initial surface adhesion leads to smaller debris being created from the asperities. It can be interpreted as a way to mimic an initial passivation of the surface.

3 Results

Effect of temperature on material properties. As the temperature rises, the material properties of the material are affected as

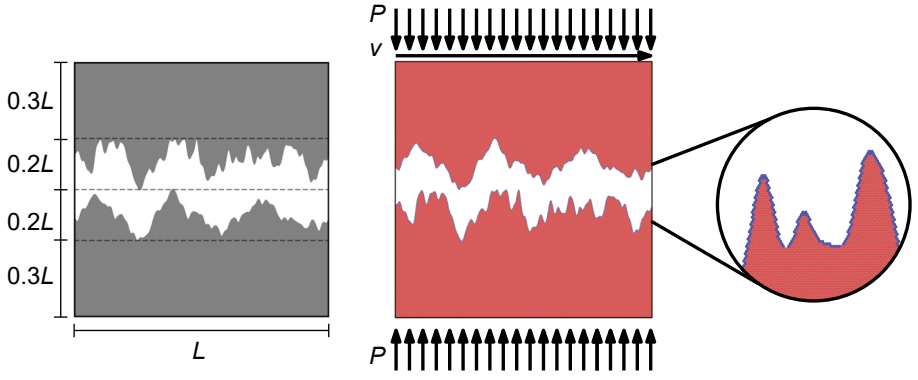

Fig. 2 Simulation domains used in the long-time frame simulation. (a) The geometry. (b) The area between the two rough surfaces removed from a regular hexagonal lattice of atoms to create the starter simulation domain. The atoms in the bulk are colored in red, and the atoms with reduced adhesion at the surface are colored in blue.

represented in Fig. 3. Thermal dilatancy causes an increase of around two percents of the equilibrium bond length over the tested temperature range. This increased spacing between atoms results in a modest reduction of the surface energy γ_{surf} by less than 1%. In the box shearing simulations, as the shear strain increases, the shear stress first also increases linearly until it reaches a peak stress. After that, it quickly falls to a plateau, as represented in the inlay of Fig. 3. Both the peak and plateau shear strength depend largely on the temperature, with the peak strength reducing almost threefold over the tested temperature range. The shear modulus is barely affected by temperature. The material properties that depends on the short-range interactions, such as the stiffness and surface energy, vary only sligthly with temperature whereas the material properties dependent on the long range interactions, such as the shear strength, are significantly reduced.

Effect of temperature on the critical junction size. The shearing of a junction results in two different behaviors depending on the temperature and junction size. Either cracks can appear at the bases of the junction, leading to the detachment of a debris particle or the junction can be "squished", sustaining large plastic deformation and leading to the closing of the gap between the surfaces. Figure 4 shows two junctions of the same size but sheared at different temperatures, leading to the brittle behavior at low temperature and ductile behavior at high temperature. To delineate the two behaviors, several simulations are run at different junction sizes and temperatures to create the map presented in Fig. 5. Each dot represents a specific couple of junction size and temperature. Each couple was run for five different realizations, and the color of the dot represents the proportion of simulations that led to debris creation. Two zones can be identified: High junction size and low temperature lead to brittle behavior, whereas high temperature and small junction size lead to ductile behavior. The two zones are not clearly delineated, instead, there is a transition zone where both behaviors coexist. This transition zone is larger for higher temperatures. These results clearly show that the ductile-to-brittle transition is also a function of temperature.

By using the temperature-dependent material properties, the critical junction size $d^*(T)$ can then be predicted at different temperatures. The blue line in Fig. 5 represents $d^*(T)$ and falls into the lower part of the transition zone. As such, a formulation of d^* that accounts for temperature-dependent shear strength can reasonably predict the lower bound of the ductile-to-brittle transition with temperature change.

Effect of the sliding velocity—short time frame. As for the effect of temperature, the influence of sliding velocity on the ductile-to-brittle transition is first studied with junction shearing simulations.

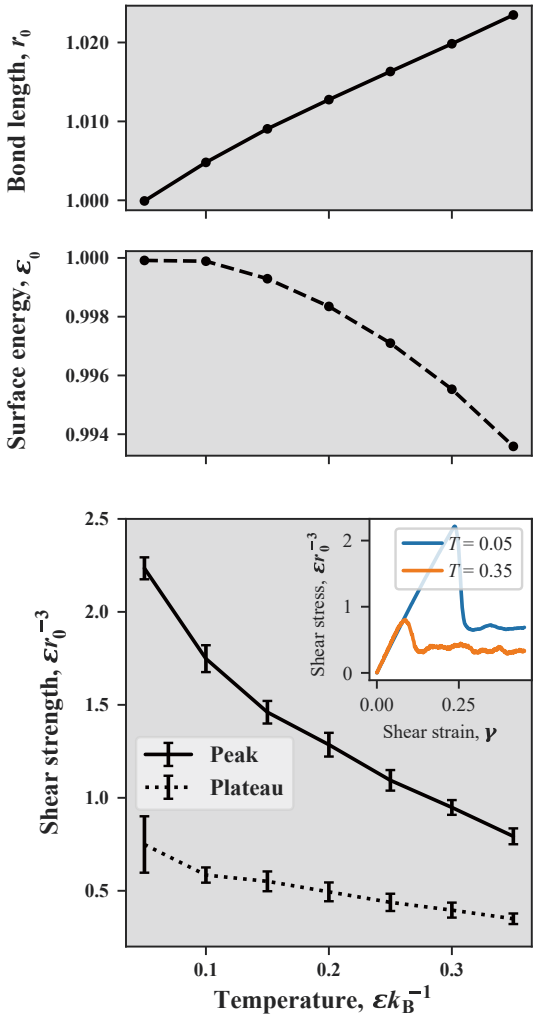

Fig. 3 Effect of raising temperature on material properties. From top to bottom, equilibrium bond length, surface energy and shear strength. Two shear strengths are measured, with one corresponding to the maximum virial shear stress attained, the other one the residual shear strength. The lines represent the mean and the error bars are the standard deviation, computed over ten realizations. In the inlay, two examples of shear stress/strain curves for temperature $T = 0.05$ and $T = 0.35$.

The junction size is fixed at $d = 15r_0$ and the initial temperature at $T = 0.2$. Then, the junction is sheared with different sliding velocities. For each sliding velocity, five realizations are run to account for the stochasticity of finite-temperature MD simulations. For low sliding velocity, both ductile and brittle

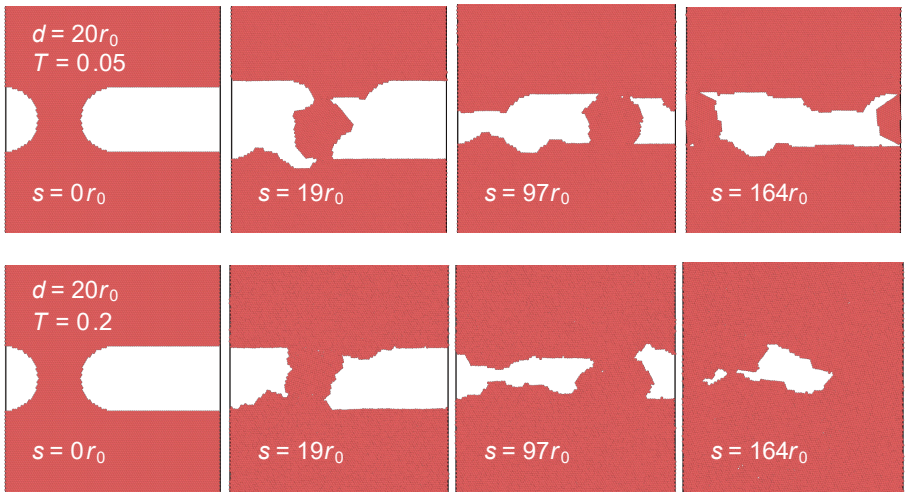

Fig. 4 Snapshots of two simulations at varying sliding distance s for the same junction size $d = 20r_0$ and different temperatures $T = 0.05$ and $T = 0.2$. At a low temperature, a rolling particle is detached from the junction and rolls between both surfaces. At a higher temperature, the junction is squished between the surfaces, which ultimately weld together.

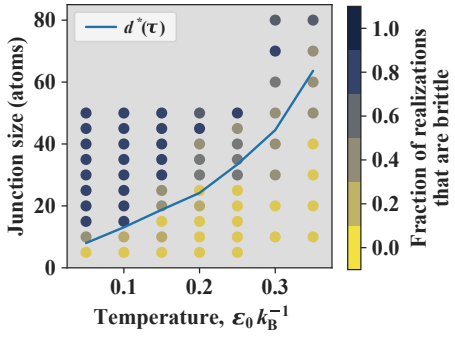

Fig. 5 Results of single asperity sliding simulations. Each point represents the average results of the five realizations at a given temperature and junction size; the shade from blue to yellow gives the proportion of simulations that lead to debris creation, as indicated by the legend on the right. The blue line corresponds to the critical junction size calculated with the temperature-dependent shear strength.

behaviors are observed; sometimes the junction fractures on its top and bottom, leading the creation of a wear particle, sometimes it sustains large plastic deformation and is squished between the surfaces. For the higher shear rate, all the simulations behave in a brittle manner. Furthermore, the junction undergoes fragmentation as shown in Fig. 6. This particularly brittle behavior is observed for sliding velocities approximately one-third of the shear wave velocity. It is clear from these simulations that the rate of loading has an impact on the observed behavior beyond the prediction of the critical junction size.

Fracture and plastic deformation usually generate heat, which can increase temperature and lead to a more ductile behavior, as shown in Fig. 5. In these short time frame simulations, the sliding is not long enough to generate a significant temperature increase as the junction is broken. Thus, longer time frame simulations are needed to complete the picture of the effect of the sliding velocity on the ductile-to-brittle transition. Such simulations are presented in the next paragraph.

Effect of the sliding velocity—long time frame. In this section, the results for the adiabatic simulations, without a thermostat, are first presented. Then, the impact of thermostating the simulations is discussed. All simulations start with the same initial roughness. As the sliding begins, the tips of the asperities make contact and break, creating particles that roll between the surfaces. These particles quickly aggregate into a single large rolling particle. The initial asperities are smoothed away, and the resulting surface

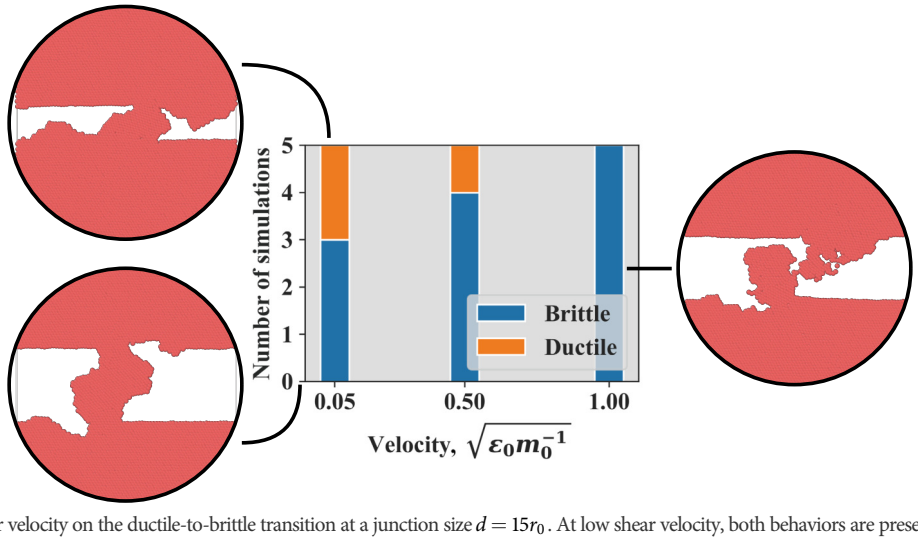

Fig. 6 Effect of the shear velocity on the ductile-to-brittle transition at a junction size $d = 15r_0$. At low shear velocity, both behaviors are present as pictured on the left. At higher velocity, not only is the behavior brittle, a fragmentation of the asperity can also be observed, as seen on the right.

清華大学出版社 Tsinghua University Press | SciOpen

roughness is smaller in amplitude. For the two higher sliding velocities, there are times when, after a collision, the gap between the two surfaces opens and the contact between them and the particle is lost. The pressure eventually put them back in contact. Figure 7 shows snapshots of the simulation sliding at medium velocity. As the sliding proceeds, the rolling particle grows and, since the boundary conditions are adiabatic, the temperature increases, as represented in Fig. 8. All simulations reach the same top temperature of approximately $T = 0.42$, which corresponds to the liquefying temperature of the material, at which point the rolling particle is squished between the surfaces. In the moments before being squished, the wear particle stops accumulating mass and its size actually decreases.

The wear process, as measured by the size of the rolling particle pictured in Fig. 8(c), happens in three phases. A first phase of high wear corresponds to the breakage of asperities and subsequent agglomeration of smaller wear particles into one large particle. In the second phase, the single aggregated wear particle rolls and accumulates mass with a constant wear rate, lower than the one of the first phase. Finally, as the temperature gets closer to the melting point, the wear slows down, and the particle even loses mass back to the surfaces. This pattern of wear, with an initial running-in, transient, period of severe wear, followed by a steady state of mild wear, is consistent with experimental observations [33–36] and past numerical investigations [14, 37, 38]. As a note regarding the initially reduced surface adhesion, the influence of reducing interfacial adhesion in a similar manner was studied in past work [39]. They concluded that reducing the adhesion did not change the minimum debris size created but, depending on the contact angle, it could increase the chance of slippage instead of breakage. As such, it can influence the distribution of initial fragment sizes. In this work, all initial fragments amalgamate quickly to form one large rolling particle, thus mitigating the influence of the initial fragment sizes.

The temperature and tangential work increase linearly with the sliding distance until liquefaction, and at almost the same rate for all three sliding velocities. In other words, the rate of heat generation is close to proportional to the sliding velocity. This can be clearly seen in Figs. 8(a) and 8(b). Both temperature and tangential work have a step pattern at the beginning of the simulation with the faster sliding velocities. The steps correspond to the collision events and the subsequent non-contact period.

When putting temperature against tangential work in Fig. 8(d), the curves for the two higher velocities superimpose, but the temperature increase is slightly higher for the same tangential work for the lower velocity. One explanation could be that, for lower velocity, contact is never lost between the particle and the two surfaces, the particle continuously rolls leading to more mechanical work being dissipated in heat and less in the fracture and deformation of asperities. This connects with previous observations that sliding velocity has little effect on wear and friction until a certain threshold is reached, above which continuous contact between the surfaces is lost and friction and wear diminish [9, 22–24]. The top velocity studied in this work might be getting close to this threshold.

The results for thermostated simulations are similar to the adiabatic case during the initial running-in and steady state phase. Figure 9 compares the growth in particle size for adiabatic and thermostated simulations. Smaller wear particles first agglomerate into a single large particle that then rolls and grows. However, as no temperature increase occurs, the wear particle does not liquefy and is not squished between the surfaces. Instead, it continues to grow.

Wear can be measured through the size of the wear particles. At the end of the first wear phase, all the smaller wear particles have agglomerated into one large particle, whose size indicates the magnitude of wear. While the trend is not clear for adiabatic simulations, the thermostated simulations show a clear correlation between the sliding velocity and the particle size. The higher the sliding velocity, the larger the wear particle after the initial running-

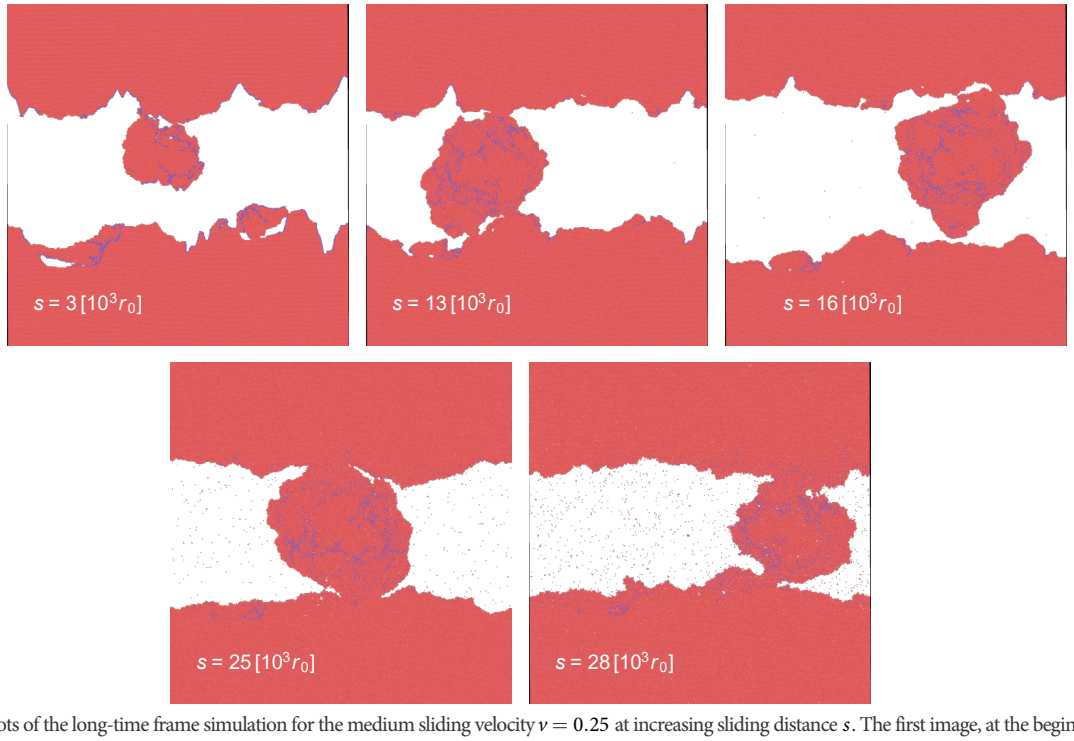

Fig. 7 Snapshots of the long-time frame simulation for the medium sliding velocity $v = 0.25$ at increasing sliding distance s. The first image, at the beginning of sliding, is at a time when all the small particles originating from broken asperities have not yet agglomerated into one large particle. The third snapshot shows a moment when contact is lost between the surfaces and the particle; the fourth is near the peak size of the particle; the last is just before the collapse of the particle.

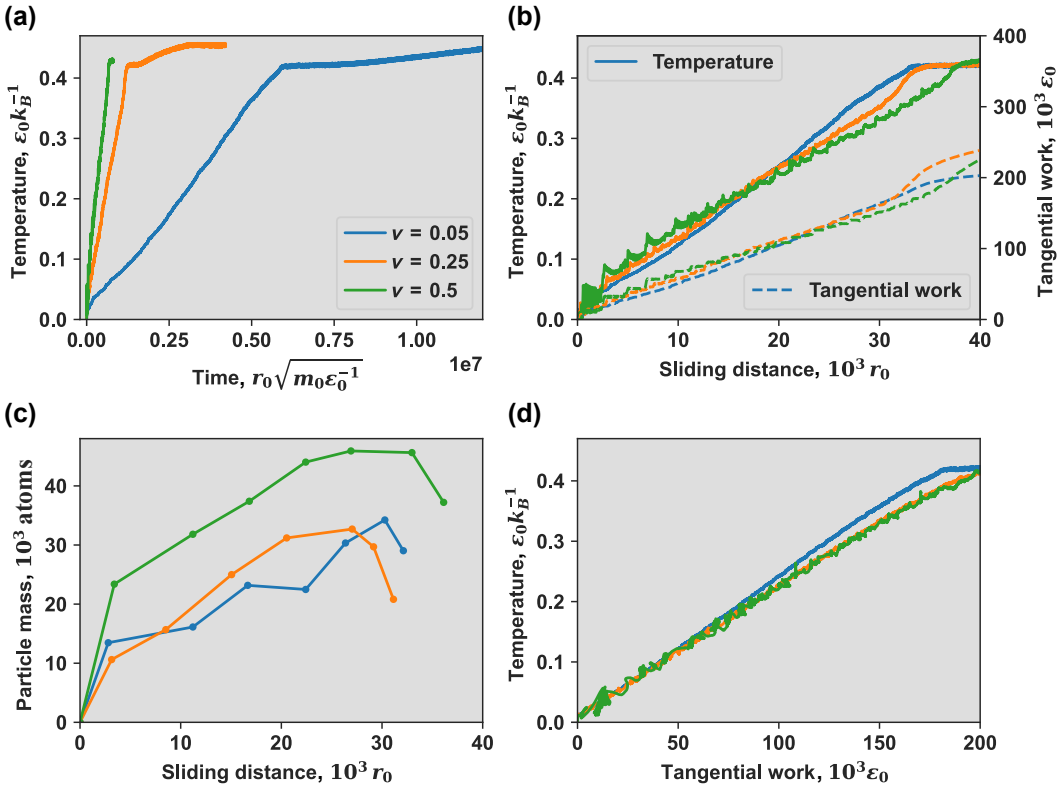

Fig. 8 Results of the three long time frame simulations in adiabatic conditions for velocity $v = 0.05$, $v = 0.25$, and $v = 0.5$. The color of the lines indicates the velocity. (a) Temperature as a function of time. (b) Temperature and tangential work as a function of sliding distance. (c) Particle mass, which is a proxy measurement of wear, as a function of sliding distance. (d) Temperature as a function of tangential work.

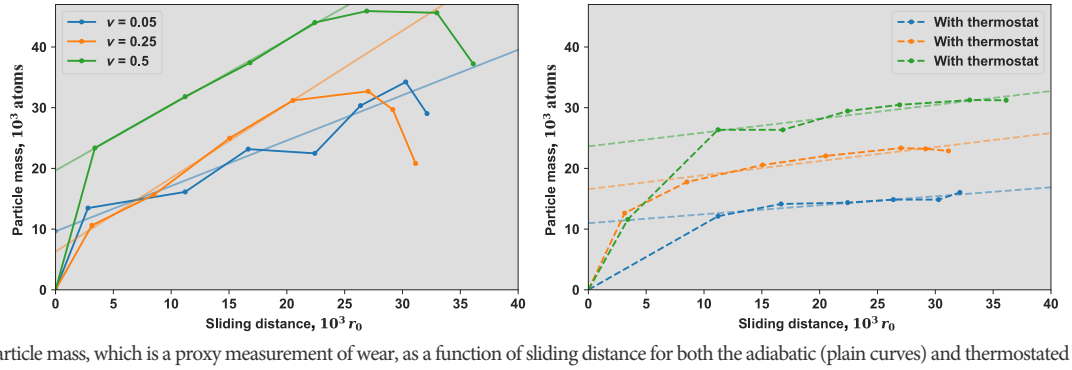

Fig. 9 Wear particle mass, which is a proxy measurement of wear, as a function of sliding distance for both the adiabatic (plain curves) and thermostated (dotted curves) simulations. The shaded lines highlight the wear rate during the second phase of wear, corresponding to a rolling particle wear mode.

in phase. This could be explained by the higher brittleness at elevated sliding velocity, which makes the tips of asperities more likely to break thus leading to more mass being agglomerated. However, the second phase, corresponding to a rolling particle wear mode, displays a constant wear rate, seemingly independent of sliding velocity. This wear rate is higher for adiabatic simulations with an average of $1\,[m_0 r_0^{-1}]$ compared to $0.2\,[m_0 r_0^{-1}]$ for thermostated simulations.

The constant wear rate observed in thermostated simulations for the second wear phase is in line with a previous numerical study of rolling wear particles [14]. For the adiabatic case, the temperature increases, leading to the shear strength being reduced by half at the end of the second wear phase (sliding distance between approximately $s = 5\,[10^3 r_0]$ to $s = 25\,[10^3 r_0]$). Given that shear strength and hardness are close to proportional, from Archard's wear law, which predicts that wear is inversely proportional to the hardness of the material [40], and the previous numerical study [14], we would be expecting to observe an increasing wear rate instead of a constant one. Further investigation would be needed to reconcile why a constant wear rate is observed in both cases despite the significant temperature increase in the adiabatic case.

From this set of simulations, we can conclude that, in both the thermostated and adiabatic conditions, the state of the interface and its behavior depend mainly on the sliding distance and not sliding time or sliding velocity, both for the running-in and steady state period. The sliding velocity has only a weak influence on tangential work, wear, and friction. However, higher sliding velocities seem to lead to more wear in the first running-in phase, especially in thermostated conditions.

4 Discussion

Plastic fracture and the critical junction size. By assuming the plastic dissipation to be zero, d^* predicts a reasonable lower bound of the ductile-to-brittle transition: It gives the point at

which not only plastic deformation is expected but also the start of the occurrence of cracks. To predict the upper bound of the transition, where fracture becomes the main mechanism of wear, a solution might be to add a term accounting for the temperature-dependent plastic dissipation γ_p to d^*.

The plastic dissipation γ_p is not only a material parameter, it also depends on the loading conditions. As such, it is not as straightforward to measure as the surface energy, the shear modulus or the shear strength. The toughness of the material, which is proportional to the square root of the product of G_c and μ, could be a proxy measurement. Experimental investigations of real materials return a breadth of behaviors: Some studies have found an increased toughness with temperature [41–43] while other materials see their toughness decrease with temperature [44–46]. How does the critical junction size d^*, and its related length scale the size of the fracture process zone [17], evolves with temperature remains an open research question.

Heat diffusion. The simulations were run either thermostated by an external heat bath or in adiabatic conditions. These represent the two limit cases where heat diffusion in the bulk is neglected. In most real applications, the heat generated at the sliding interface could also diffuse through the bulk. In this case, the different rates of heat generation with varying sliding velocities would result in different temperature profiles. Figure 10 shows a simple model of heat diffusion in a finite medium of depth L with a heat source at the interface. The temperature increase is proportional to the heat source rate and the distance to the fixed temperature boundary:

$$\Delta T = T_{\max} - T_0 = \dot{Q}L \propto vL \tag{6}$$

As the heat generation rate depends on the sliding velocity, the temperature profile and peak temperature also depend on the sliding velocity. Higher sliding velocity would lead to higher temperatures at the interface, leading to a more ductile behavior. This effect could be counteracted by strain rate effects leading to a more brittle behavior at higher sliding velocity, as observed in the short time frame simulations. However, this case was not studied here as atomistic simulations of small scales are not appropriate to study heat diffusion. Indeed, at this scale, heat propagation is not only diffusive but also ballistic [47, 48]. Studying the effect of heat diffusion would require either using another simulation method or complementing the atomistic simulation with a continuum model of heat diffusion. While this option is out of the scope of the current work, it is a promising direction for future work.

5 Conclusions

The material studied becomes more ductile with increasing temperature as evidenced by the higher critical junction size. By measuring the shear strengths at different temperatures and using those to compute d^*, it is possible to estimate the critical junction size at different temperatures. While the predictions are relatively close to the observed ductile-to-brittle transition, the current formulation of d^* tends to underpredict and is closer to the lower bound of the transition. This might be due to the assumption of a perfectly brittle material in the current formulation of d^*. For ductile materials, the critical energy release rate should include the energy dissipated as plastic strain near the crack tip. This energy dissipation is temperature-dependent and could correct the underprediction of d^*.

The sliding velocity also influences the brittle-to-ductile transition. At higher shear rates, a new brittle mode of fracture is observed: fragmentation. As no term in d^* is dependent on the shear rate, it cannot predict this effect. How to include the effect of the sliding velocity in the prediction of the ductile-to-brittle transition remains an open question.

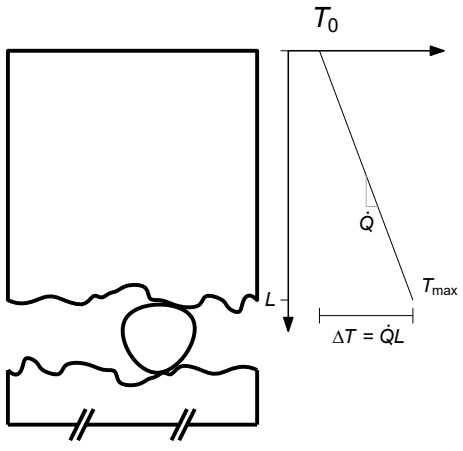

Fig. 10 Steady state solution of the temperature profile with a heat source $\dot{Q}$ at the sliding interface and a fixed temperature T_0 at a distance L.

Finally, simulations of rough-on-rough surfaces sliding match experimental observations for the wear rate pattern. In those longer time frame simulations, sliding velocity has little impact on heat generation, tangential work or wear rate in most cases, the main predictor being the sliding distance. The only clear influence of velocity is a higher amount of wear in the first running-in phase. One caveat is that the conditions were either thermostated or adiabatic. In most tribosystems, heat generated at the sliding interface will also diffuse in the bulk, at which point heat generation rate, and thus sliding velocity, is expected to have a more significant effect on the tribological behavior and the ductile-to-brittle transition.

Appendix Domain size justification

Shear strength simulations. The domain is a square box of width and height of 100 atoms. The shear strength is indeed dependent on the size of the box considered, see Ref. [13], Fig. 2(a). Smaller box sizes lead to higher shear strength. For boxes with sides larger than 50 atoms, the shear strength plateaus. In this work, the size of the box, 100-atom large, is big enough to avoid this size effect.

Critical junction size and short time frame velocity effect simulations. The size of the domain scales with the junction size as indicated in Fig. 1(b).

Here, we have to distinguish between the lateral periodic boundaries and the ones on the top and bottom where pressure and velocity are enforced.

For the lateral boundaries, having them too close to the junction could result in the asperity interacting with itself due to the periodic condition. This effect of asperity interaction was studied in Ref. [50]. It was found that a combined behavior can happen only if

$$d_a \leq d^2/d^* \tag{7}$$

with d_a the apparent surface area and d the junction size. In the simulations, since the domain size scales with the junction size, we have $d_a = 6d_r$. As such, asperity interaction could happen only if the simulated junction size is six times larger than the critical junction size. The only simulations close to this criterion are the ones run at a low temperature of $T = 0.05$. For this temperature, d^* was found to be approximately $10 \pm 5r_0$. Then, simulations with a junction size $d > 30r_0$ could be at risk of asperity interaction. While these simulations could easily be removed from

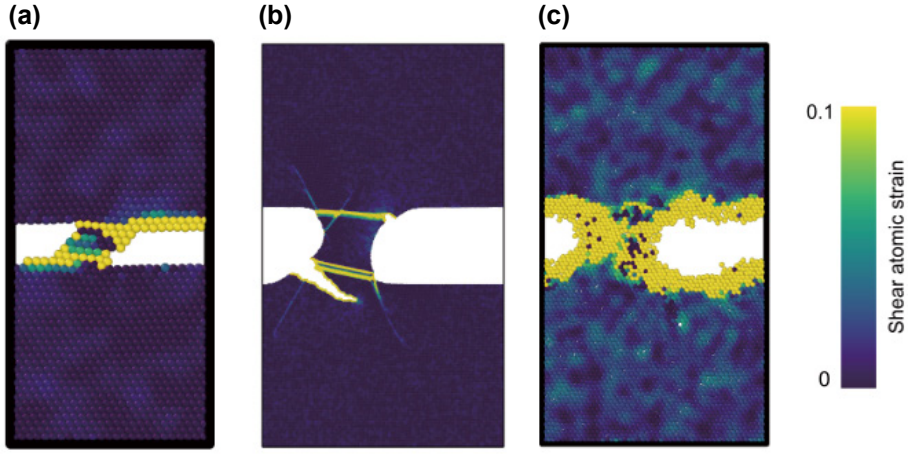

Fig. 11 Shear atomic strain for three edge cases: (a) with $T = 0.05$ and $d = 5$, (b) with $T = 0.05$ and $d = 50$, and (c) with $T = 0.35$ and $d = 10$. The large atomic strains are far removed from the top and botton boundaries. The noise is due to non-zero temperature. For (c), the whole free surfaces suffer from large strain because, due to the high temperature, the surface atoms are detaching and flying away.

the results without changing in any way the conclusion of the manuscript, a visual inspection of the results clearly shows that no such interaction happens.

For the top and bottom boundary, it can be checked that the strains are concentrated near the asperity, and dislocations stop far from the boundaries. Example cases are illustrated in Fig. 11.

Concerning the thermostat layer situated at the top and bottom boundaries, their reference temperature is corrected for rigid body motion so that they do not create virtual viscous forces. It can be verified that the temperature of the system is maintained at the expected one as can be seen in Fig. 12.

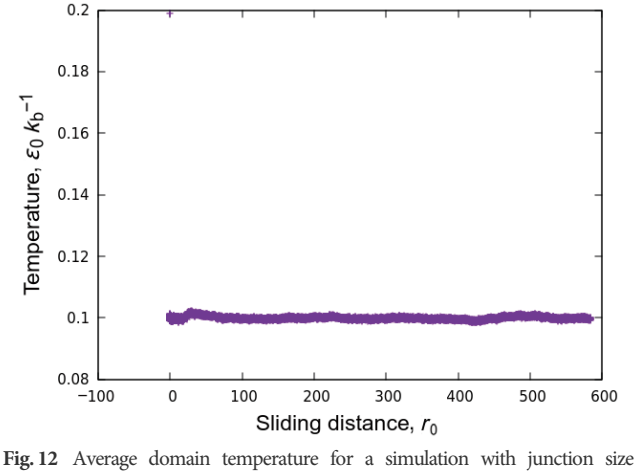

Fig. 12 Average domain temperature for a simulation with junction size $d = 50$ and initial temperature and thermostat set at $T = 0.1$.

Long time frame adiabatic simulations. The domain is a square box of width and height of 500 atoms. Given the adiabatic conditions, increasing the domain height would increase the total thermal mass to heat up but would not change the intensity of the heat source. As such, it is expected that it would slow the increase in temperature.

For the size of the box, a similar argument as above can be made.

Declaration of competing interest

The authors have no competing interests to declare that are relevant to the content of this article.

Acknowledgments

This work was supported by the Swiss National Science Foundation under the grant "Wear across scales" (197152).

Data availability

All data to reproduce the results presented here are openly available at https://doi.org/10.5281/zenodo.18643018.

References

[1] Tao Z, Bhushan B. Surface modification of AFM silicon probes for adhesion and wear reduction. *Tribol Lett* **21**(1): 9001 (2006)
[2] Gotsmann B, Lantz M A. Atomistic wear in a single asperity sliding contact. *Phys Rev Lett* **101**(12): 125501 (2008)
[3] Merkle A P, Marks L D. Liquid-like tribology of gold studied by *in situ* TEM. *Wear* **265**(11–12): 1864–1869 (2008)
[4] Liu J, Notbohm J K, Carpick R W, Turner K T. Method for characterizing nanoscale wear of atomic force microscope tips. *ACS Nano* **4**(7): 3763–3772 (2010)
[5] Sato T, Ishida T, Jalabert L, Fujita H. Real-time transmission electron microscope observation of nanofriction at a single Ag asperity. *Nanotechnology* **23**(50): 505701 (2012)
[6] Vahdat V, Grierson D S, Turner K T, Carpick R W. Mechanics of interaction and atomic-scale wear of amplitude modulation atomic force microscopy probes. *ACS Nano* **7**(4): 3221–3235 (2013)
[7] Jacobs T D B, Carpick R W. Nanoscale wear as a stress-assisted chemical reaction. *Nature Nanotech* **8**(2): 108–112 (2013)
[8] Chung K H. Wear characteristics of atomic force microscopy tips: A review. *Int J Precis Eng Man* **15**(10): 2219–2230 (2014)
[9] Bhushan B, Sundararajan S. Micro/nanoscale friction and wear mechanisms of thin films using atomic force and friction force microscopy. *Acta Mater* **46**(11): 3793–3804 (1998)
[10] Chung K H, Kim D E. Fundamental investigation of micro wear rate using an atomic force microscope. *Tribol Lett* **15**(2): 135–144 (2003)
[11] Aghababaei R, Warner D H, Molinari J F. Critical length scale controls adhesive wear mechanisms. *Nat Commun* **7**: 11816 (2016)
[12] Aghababaei R, Brink T, Molinari J F. Asperity-level origins of transition from mild to severe wear. *Phys Rev Lett* **120**(18): 186105 (2018)
[13] Wattel S Z, Garcia-Suarez J, Molinari J F. Understanding the mechanisms of adhesive wear for heterogeneous materials through atomistic simulations. *Extreme Mech Lett* **57**: 101913 (2022)
[14] Wattel S Z, Molinari J F. A story of two transitions: From adhesive to abrasive wear and from ductile to brittle regime. *J Chem Phys* **160**: 014711 (2024)
[15] Aghababaei R, Malekan M, Budzik M. Cutting depth dictates the

transition from continuous to segmented chip formation. *Phys Rev Lett* **127**(23): 235502 (2021)
[16] Zheng W, Ma L, Pei S, Aghababaei R. Numerical assessment of transition in cutting mode and its effect on roughness creation. *Int J Mech Sci* **261**: 108666 (2024)
[17] Garcia-Suarez J, Brink T, Molinari J F. Breakdown of Reye's theory in nanoscale wear. *J Mech Phys Solids* **173**: 105236 (2023)
[18] Zhao K, Aghababaei R. Adhesive wear law at the single asperity level. *J Mech Phys Solids* **143**: 104069 (2020)
[19] Frérot L, Aghababaei R, Molinari J F. A mechanistic understanding of the wear coefficient: From single to multiple asperities contact. *J Mech Phys Solids* **114**: 172–184 (2018)
[20] Brink T, Frérot L, Molinari J F. A parameter-free mechanistic model of the adhesive wear process of rough surfaces in sliding contact. *J Mech Phys Solids* **147**: 104238 (2021)
[21] Persson B N J, Xu R, Miyashita N. Rubber wear: Experiment and theory. *J Chem Phys* **162**(7): 074704 (2025)
[22] Yang Y, O'Hern C S, Huang L, Shi Y. The nature of atomic wear from molecular simulations. *Tribol Int* **167**: 107418 (2022)
[23] Sun J, Yuan Z, Zheng P, Tang M, Wang Y, Sun X, He Y. Study on the microscopic wear mechanism of nanoparticles sliding stainless steel. *Model Simul Mater Sc* **31**(6): 065010 (2023)
[24] Raghuraman S, Boonpuek P, King K H, Ye Z, Felts J R. The role of speed in atomic scale wear. *J Phys Chem C* **125**(7): 4139–4145 (2021)
[25] Thompson A P, Aktulga H M, Berger R, Bolintineanu D S, Brown W M, Crozier P S, in 't Veld P J, Kohlmeyer A, Moore S G, Nguyen T D, et al. LAMMPS—A flexible simulation tool for particle-based materials modeling at the atomic, meso, and continuum scales. *Comput Phys Commun* **271**: 108171 (2022)
[26] Rajan V P, Warner D H, Curtin W A. An interatomic pair potential with tunable intrinsic ductility. *Model Simul Mater Sc* **24**(2): 025005 (2016)
[27] Aghababaei R, Warner D H, Molinari J-F. On the debris-level origins of adhesive wear. *P Natl Acad Sci USA* **114**(30): 7935–7940 (2017)
[28] Shinoda W, Shiga M, Mikami M. Rapid estimation of elastic constants by molecular dynamics simulation under constant stress. *Phys Rev B* **69**(13): 134103 (2004)
[29] Tuckerman M E, Alejandre J, López-Rendón R, Jochim A L, Martyna G J. A Liouville-operator derived measure-preserving integrator for molecular dynamics simulations in the isothermal–isobaric ensemble. *J Phys A—Math Gen* **39**(19): 5629–5651 (2006)
[30] Rey V, Anciaux G, Molinari J F. Normal adhesive contact on rough surfaces: Efficient algorithm for FFT-based BEM resolution. *Comput Mech* **60**(1): 69–81 (2017)
[31] Frérot L, Bonnet M, Molinari J F, Anciaux G. A Fourier-accelerated volume integral method for elastoplastic contact. *Comput Meth Appl M* **351**: 951–976 (2019)
[32] Thom C A, Brodsky E E, Carpick R W, Pharr G M, Oliver W C, Goldsby D L. Nanoscale roughness of natural fault surfaces controlled by scale -dependent yield strength. *Geophys Res Lett* **44**(18): 9299–9307 (2017)
[33] Queener C A, Smith T C, Mitchell W L. Transient wear of machine parts. *Wear* **8**(5): 391–400 (1965)
[34] Chiou Y C, Kato K, Kayaba T. Effect of normal stiffness in loading system on wear of carbon steel: Part 1: Severe-mild wear transition. *J Tribol* **107**(4): 491–495 (1985)
[35] Wang W, Scholz C H. Wear processes during frictional sliding of rock: A theoretical and experimental study. *J Geophys Res* **99**(B4): 6789–6799 (1994)
[36] Bhushan B. *Modern Tribology Handbook*. Boca Raton (USA): CRC Press, 2000.
[37] Milanese E, Brink T, Aghababaei R, Molinari J F. Emergence of self-affine surfaces during adhesive wear. *Nat Commun* **10**: 1116 (2019)
[38] Milanese E, Brink T, Aghababaei R, Molinari J F. Role of interfacial adhesion on minimum wear particle size and roughness evolution. *Phys Rev E* **102**(4): 043001 (2020)
[39] Brink T, Molinari J F. Adhesive wear mechanisms in the presence of weak interfaces: Insights from an amorphous model system. *Phys Rev Mater* **3**(5): 053604 (2019)
[40] Archard J F. Contact and rubbing of flat surfaces. *J Appl Phys* **24**(8): 981–988 (1953)
[41] Nakao S, Ando T, Shikida M, Sato K. Effect of temperature on fracture toughness in a single-crystal-silicon film and transition in its fracture mode. *J Micromech Microeng* **18**(1): 015026 (2008)
[42] Feng G, Kang Y, Meng T, Hu Y Q, Li X H. The influence of temperature on mode I fracture toughness and fracture characteristics of sandstone. *Rock Mech Rock Eng* **50**(8): 2007–2019 (2017)
[43] Jia R, Zeng W, He S, Gao X, Xu J. The analysis of fracture toughness and fracture mechanism of Ti60 alloy under different temperatures. *J Alloys Compd* **810**: 151899 (2019)
[44] Banea M D, da Silva L F M, Campilho R D S G. Effect of temperature on tensile strength and mode I fracture toughness of a high temperature epoxy adhesive. *J Adhes Sci Technol* **26**(7): 939–953 (2012)
[45] Neuman E W, Hilmas G E, Fahrenholtz W G. Mechanical behavior of zirconium diboride–silicon carbide ceramics at elevated temperature in air. *J Eur Ceram Soc* **33**(15–16): 2889–2899 (2013)
[46] Neuman E W, Hilmas G E, Fahrenholtz W G. Mechanical behavior of zirconium diboride–silicon carbide–boron carbide ceramics up to 2200 °C. *J Eur Ceram Soc* **35**(2): 463–476 (2015)
[47] Kittel C. *Introduction to Solid State Physics*. Weinheim (Germany): Wiley, 2004.
[48] Anciaux G, Molinari J F. A molecular dynamics and finite elements study of nanoscale thermal contact conductance. *Int J Heat Mass Transf* **59**: 384–392 (2013)
[49] Jacobson D W, Thompson G B. Revisting lennard Jones, morse, and N-M potentials for metals. *Comput Mater Sci* **205**: 111206 (2022)
[50] Pham-Ba S, Brink T, Molinari J F. Adhesive wear and interaction of tangentially loaded micro-contacts. *Int J Solids Struct* **188–189**: 261–268 (2020)

Sacha Zenon Wattel, Ph.D., completed his Ph.D. degree under the guidance of Professor Molinari, delving into the world of numerical nano tribology to uncover the fundamental mechanics that drive wear and friction.

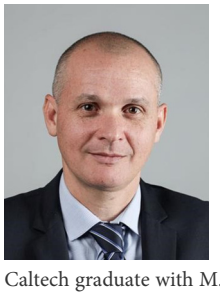

Jean-François Molinari, professor, directs the Computational Solid Mechanics Laboratory at Ecole Polytechnique Fédérale de Lausanne (EPFL), where he holds appointments in civil engineering and materials science. He joined EPFL in 2007, became a full professor in 2012, and previously led the Civil Engineering Institute. He serves on the Research Council of the Swiss National Science Foundation and is co-editor in chief of *Mechanics of Materials*. A Caltech graduate with M.S. and Ph.D. degrees in aeronautics, he has held academic positions at Johns Hopkins University, École Normale Supérieure Cachan, and École Polytechnique de Paris. His research spans multiscale modeling, damage mechanics, nano- and microstructural properties, and tribology.